

# Macromolecular Materials and Engineering

## Epoxy doped, nanoscale phase-separated poly-acrylates with potential in 3-D printing

--Manuscript Draft--

<b>Manuscript Number:</b>	mame.202000558R2
<b>Article Type:</b>	Full Paper
<b>Corresponding Author:</b>	Osman Konuray, Ph.D. Universitat Politecnica de Catalunya Barcelona, Catalonia SPAIN
<b>Corresponding Author E-Mail:</b>	ali.osman.konuray@upc.edu
<b>Order of Authors:</b>	Osman Konuray, Ph.D. Arnau Altet Jordi Bonada Agnieszka Tercjak Xavier Fernández-Francos Xavier Ramis
<b>Keywords:</b>	Additive Manufacturing; 3D Printing; epoxy-anhydride; IPN
<b>Section/Category:</b>	
<b>Abstract:</b>	<p>An efficient method to improve the mechanical performance of a commercially available photocure resin is described wherein the resin is modified with a mixture of a cycloaliphatic epoxy and an anhydride curing agent. Photocured samples are thermally treated in a subsequent step to cure the epoxy to obtain an interpenetrated polymer network (IPN) and also complete reaction of the acrylate monomers remaining from the photocure. The latter is accomplished by a thermal radical initiator added earlier into the formulation together with the epoxy-anhydride. The thermal properties and microstructure of the resulting IPN are analyzed. Uniform and quantitative conversions are obtained, with glass transition temperatures comparable to conventional epoxies. The liquid, uncured samples containing different amounts of epoxy are stable at 30°C for several weeks. In the fully cured epoxy-rich materials, nano-scale phase separation is observed by AFM. This is corroborated by the existence of multiple relaxations determined by DMA analysis. Specimens from a formulation containing 50% by weight of epoxy-anhydride are 3D printed in a customized Masked Image Processing Stereolithography (MIP-SL), thermally treated, and are subjected to compression tests. Results show that the Young's modulus increases by 900% over the neat resin.</p>
<b>Author Comments:</b>	
<b>Additional Information:</b>	
<b>Question</b>	<b>Response</b>
Please submit a plain text version of your cover letter here.	<p>Dear editor,</p> <p>We hereby submit our revised manuscript titled "Epoxy doped, nanoscale phase-separated poly-acrylates with potential in 3-D printing" to be considered for publication in Macromolecular Materials and Engineering as a Full Article.</p> <p>We have taken the reviewer comments into consideration and applied the suggested minor changes. Attached to this submission, find our responses to their comments.</p> <p>Sincerely,</p> <p>Dr. Osman Konuray (on behalf of all authors)</p>

Do you or any of your co-authors have a conflict of interest to declare?	No. The authors declare no conflict of interest.
<b>Response to Reviewers:</b>	

Dear reviewer,  
We thank you once again for your feedback. Find our responses below.  
Best regards,  
Dr. Osman Konuray (on behalf of all authors)

Reference 18 does not appear to be correct. The citation in the text states: "similar to what was previously reported for similar acrylate-epoxy interpenetrated polymer networks (IPNs)." But the cited paper appears to be on epoxy-thiol systems.

I think the reference list in the revised manuscript has not been updated with the new added references as there are only 21 references but there are at least 24 citations in the revised version. Did not check all citations but this would explain the inconsistency noted above.

The reviewer is correct. We had simply forgotten to update our reference list after the changes. We have corrected it in this new version.

Pg 23: "At this point, onc can doubt..." (one can doubt...)

Typo is corrected.

Page 30: "Since the amount of initiators were small, they were added primarily to glass vials..."

I would recommend replacing "primarily" with "first" as primarily can also mean 'for the most part' or 'mainly' which is not what the authors wish to convey. "Since the amount of initiators were small they were added first to glass vials..."

We agree that "first" is more suitable. The change was applied.

## **Epoxy doped, nanoscale phase-separated poly-acrylates with potential in 3-D printing**

*Osman Konuray\**, *Arnau Altet*, *Jordi Bonada*, *Agnieszka Tercjak*, *Xavier Fernández-Francos*,  
*Xavier Ramis*

Dr. O. Konuray, A. Altet, Dr. X. Fernández-Francos, Prof. X. Ramis  
Thermodynamics Laboratory, ETSEIB. Universitat Politècnica de Catalunya, Avda. Diagonal  
647, 08028 Barcelona, Spain.  
E-mail : ali.osman.konuray@upc.edu

Dr. J. Bonada  
Strength of Materials and Structural Engineering, ETSEIB, Universitat Politècnica de  
Catalunya, Avda. Diagonal 647, 08028 Barcelona, Spain

Dr. A. Tercjak  
Group ‘Materials + Technologies’, Polytechnic School, Dpt. of Chemical Engineering and  
Environment, Universidad País Vasco/Euskal Herriko Unibertsitatea, Pza. Europa 1, 20018  
Donostia-San Sebastián, Spain

Keywords: additive manufacturing, 3D printing, epoxy-anhydride, IPN

An efficient method to improve the mechanical performance of a commercially available photocure resin is described wherein the resin is modified with a mixture of a cycloaliphatic epoxy and an anhydride curing agent. Photocured samples are thermally treated in a subsequent step to cure the epoxy to obtain an interpenetrated polymer network (IPN) and also complete reaction of the acrylate monomers remaining from the photocure. The latter is accomplished by a thermal radical initiator added earlier into the formulation together with the epoxy-anhydride. The thermal properties and microstructure of the resulting IPN are analyzed. Uniform and quantitative conversions are obtained, with glass transition temperatures comparable to conventional epoxies. The liquid, uncured samples containing different amounts of epoxy are stable at 30°C for several weeks. In the fully cured epoxy-rich materials, nano-scale phase separation is observed by AFM. This is corroborated by the existence of multiple relaxations determined by DMA analysis. Specimens from a formulation containing 50% by weight of epoxy-anhydride are 3D printed in a customized Masked Image Processing Stereolithography (MIP-SL), thermally treated, and are subjected to compression tests. Results show that the Young’s modulus increases by 900% over the neat resin.

### **1. Introduction**

Apart from its well established utility in prototyping, additive manufacturing (AM, or more popularly, 3D printing) is becoming the method of choice for the manufacturing industry,

1 replacing conventional production processes in applications such as biomedical materials <sup>1,2</sup>,  
2 soft robotics <sup>2</sup>, machinery parts <sup>3</sup>, and sports goods. <sup>4,5</sup> In general, the photocurable resins for  
3 3D printing are required to have low viscosities. The parts are printed layer-by-layer (along the  
4 z-axis) by photocuring each layer (over the x-y plane) using a laser beam (in SLA) or a digital  
5 image projection of the cross-section (in DLP).  
6  
7  
8  
9

10 Often times, the photopolymerization technology is either based on free-radical or cationic  
11 initiation, for which the photopolymerizable resin is usually of acrylic or epoxide origin,  
12 respectively. <sup>6-8</sup> Each technology has its advantages and disadvantages. Although the free-  
13 radical mechanism is the faster one, it suffers from oxygen inhibition and polymerization  
14 induced shrinkage, unless one benefits from the former by a special printer configuration which  
15 involves a dead zone between the printed part and the resin vat bottom. <sup>5</sup> Moreover, the printed  
16 parts are brittle and thus inadequate for applications requiring mechanical performance. Using  
17 a cationic mechanism, these drawbacks can mostly be alleviated, but one would suffer from  
18 lower reaction rates and conversions. <sup>8-10</sup> Therefore, an optimal strategy is to adopt a hybrid  
19 method, formulating a 3D printable resin that contains both acrylate and epoxide monomers.  
20 Needless to say, the incorporation of an epoxy network would also enhance mechanical  
21 properties of the printed material. Many such novel hybrid 3D printed materials were described  
22 in recent polymer literature. At any rate, the curing process is either completed in the printer by  
23 photopolymerizing both monomers simultaneously <sup>6,8,11</sup>, or by using a two-stage, sequential  
24 process. <sup>12-15</sup>  
25  
26  
27  
28  
29  
30  
31  
32  
33  
34  
35  
36  
37  
38  
39

40 In this work, we utilize a custom-made Mask Image Projection based on stereolithography  
41 (MIP-SL) printer. The working principle of this printer shares features with both SLA and DLP  
42 configurations. Whereas the platform that carries the printed part sinks into the vat as the layers  
43 are printed (as in a SLA machine), each layer is printed by projecting the corresponding cross-  
44 section image using a visible light projector. The reader is referred to our earlier work for  
45 specifics of this printer setup. <sup>13,16</sup> As with any 3D printing method that relies on  
46 photopolymerization, some problems must be considered, such as the occurrence of spatial  
47 conversion gradients (due to inhomogeneous irradiation). Although a UV post-curing stage can  
48 partially mitigate this problem, curing schedules should be planned so as to avoid these spatial  
49 gradients along part dimensions and minimize deformation, cracking, or delamination. <sup>16,17</sup>  
50  
51  
52  
53  
54  
55  
56  
57  
58  
59  
60  
61  
62  
63  
64  
65

1 thermal curing of the epoxy-anhydride. Compared to the other papers mentioned, the novelty  
2 of the work is twofold: the utilization of visible light in lieu of UV irradiation, and the use of a  
3 thermally triggered radical initiator which ensures that all remaining acrylate monomers end up  
4 polymerizing at the thermal stage, concurrently with epoxy-anhydride reaction. Needless to say,  
5 a visible light projector is more readily available and is less costly than a UV lamp. As a matter  
6 of fact, we used a home-type digital projector adapted to our custom MIP-SL configuration.  
7 Finally, going further in our analysis, we establish a nano-scale phase separation in the printed  
8 materials, similar to what was previously reported for similar acrylate-epoxy interpenetrated  
9 polymer networks (IPNs).<sup>18</sup> Such phase separation, with one phase having significantly higher  
10 glass transition temperature ( $T_g$ ), might prove useful in certain applications in which materials  
11 are required to retain their storage moduli at high temperatures.  
12  
13  
14  
15  
16  
17  
18  
19  
20

## 21 **2. Results and Discussion**

### 22 **2.1. Curing kinetics**

23  
24  
25  
26 The curing process of the hybrid formulations was monitored using DSC and FTIR as explained  
27 in the experimental section. Quantitative conversions were achieved at each stage and overall.  
28 In the interpenetrated configuration, hydrogen bonding interactions such as those indicated in  
29 **Figure 1** would help to compatibilize the two different polymeric structures as was documented  
30 previously.<sup>13</sup> As can be seen, such H-bonding is possible not only within the urethane acrylate  
31 network itself, but also between the epoxy and urethane acrylate networks.  
32  
33  
34  
35  
36

37 As proof of concept, we cured the HT50CEMA50 formulation in a thermal DSC scan and  
38 compared its second curing (epoxy-anhydride) stage with another sample whose first stage  
39 (acrylate polymerization) had been completed under UV irradiation in DSC. As can be seen in  
40 the DSC thermogram given in **Figure 2**, the first peak corresponds to radical polymerization of  
41 acrylates (facilitated thermally by LUP), and the second peak corresponds to epoxy-anhydride  
42 copolymerization. By integration of the peaks, reaction heats were found to be equal to that of  
43 pure HT100 and CEMA100 which were reported in earlier works<sup>13,19</sup>, thereby confirming the  
44 reactions. The two stages are clearly separated by temperature, even in a purely thermal process,  
45 which implies that once stage 1 is completed, the material will be chemically stable as long as  
46 the temperature is maintained below 100 °C. A formal storage stability analysis will also be  
47 presented towards the end of the article.  
48  
49  
50  
51  
52  
53  
54  
55  
56

57 An isothermal FTIR analysis of the dual-curing process was also performed. The acrylate,  
58 anhydride and epoxy absorption bands changed as expected. All characteristic acrylate peaks  
59  
60  
61  
62  
63  
64  
65

1  
2  
3  
4  
5  
6  
7  
8  
9  
10  
11  
12  
13  
14  
15  
16  
17  
18  
19  
20  
21  
22  
23  
24  
25  
26  
27  
28  
29  
30  
31  
32  
33  
34  
35  
36  
37  
38  
39  
40  
41  
42  
43  
44  
45  
46  
47  
48  
49  
50  
51  
52  
53  
54  
55  
56  
57  
58  
59  
60  
61  
62  
63  
64  
65

disappeared after Stage 1 (**Figure 3**, top), leaving anhydride and epoxy peaks intact, which disappeared after Stage 2 (Figure 3, bottom).

A detailed kinetic analysis of this two-step process will be published in a separate paper. The conversion time data obtained by different techniques (isothermal FTIR and DSC) are in accordance as illustrated in **Figure 4**, showing the absolute conversion  $x_{abs}$  calculated using Equation E1 (Experimental section). Note that for this HT50CEMA50 formulation, the weighing factor  $f_l$  will be equal to 0.5. Looking at Figure 4, one can appreciate the rapid photocuring step which is completed in mere seconds. This high reaction rate is beneficial for fast 3D printing. Once the temperature is raised to 170 °C, epoxy-anhydride condensation is commenced at a moderate rate. At this temperature, full conversion is achieved in ca. 20 min.

Finally, in order to test the contribution of LUP in the homogeneity of cure, a 1,5mm rectangular prism (similar to our DMA specimens) was printed and spectra of its top and bottom surfaces were taken. In **Figure 5**, these spectra are given together with that of the uncured and fully cured material. As indicated by the difference between the top and bottom spectra, conversion along the z-axis in a 3D printed part is not uniform. One can increase irradiation time per layer to remedy this, but that would lead to impractically long printing times. As can be seen, if LUP is used, quantitative acrylate conversions are achieved overall (spectra taken at the top surface). At this point, one can doubt the utility of LUP and suggest that during thermal treatment of the printed sample, mobility restrictions would be overcome and acrylate conversion could be driven forward even in the absence of LUP. In DSC scans, whereas no residual polymerization heat was measured in printed samples from the pristine HT100 (no LUP) even at 250°C, an appreciable amount of residual polymerization heat was measured (with an onset temperature of 120°C) in LUP containing HT100 samples (See **Figure S2** in supporting information), demonstrating the utility of LUP. This result is in agreement with our previous studies with a similar dual-curing system.<sup>13</sup>

Printed objects with the new formulation are virtually the same as their neat acrylate counterparts. As can be seen in **Figure 6**, the print layers are distinguishable, typical of all layer-by-layer AM methods. The red color was achieved by adding an azo red dye to the liquid resins prior to printing. The parts darken upon thermal treatment with no deformation or loss of detail.

## 2.2. Thermal Properties

In this section, we discuss thermal-mechanical properties of the intermediate materials (immediately after stage 1 curing) and final materials. One would expect that the  $T_g$  of final materials increase with increasing CEMA percentage in the formulation, due to the higher rigidity of the epoxy-anhydride network.<sup>19</sup> With respect to crosslinking density, there should not be any significant differences among the different formulations, since both the acrylate and epoxy-anhydride networks have significant crosslinking densities, as a result of the high functionality of the acrylate and epoxy monomers.

We use the Fox expression (Equation 1) to analyze how the composition affects the  $T_g$  of the intermediate and final materials. If one is interested in predicting intermediate  $T_g$ ,  $w_1$  represents the weight fraction of the acrylate component,  $T_{g,1}$  is the glass transition temperature of the fully cured neat acrylate material, and  $T_{g,2}$  is the glass transition temperature of the uncured neat epoxy-anhydride formulation. Similarly, if the final  $T_g$  is being predicted,  $w_1$  is the weight fraction of the acrylate, and  $T_{g,1}$  and  $T_{g,2}$  represent the glass transition temperatures of the fully-cured acrylate and epoxy-anhydride networks, respectively.

$$\frac{1}{T_g} = \frac{w_1}{T_{g,1}} + \frac{(1-w_1)}{T_{g,2}} \quad (1)$$

Using the experimental  $T_g$  determined by DSC, we can plot the experimental and predicted values as in **Figure 7**. As can be seen, a wide range of  $T_g$  can be obtained, from -59 to 52 °C in intermediate materials, and from 52 to 229°C in final materials. It is quite common for dual-curing systems that intermediate materials reach gel point or not, depending on the feed ratio and functionality of the monomers contributing to the different curing stages.<sup>20</sup> However, for 3D printing, one would require a gel at the end of stage 1 regardless of the composition. Even though the gel point was not determined experimentally, it is established in literature that acrylic networks gel fairly quickly, at conversions in the range of 0.05 and 0.2.<sup>21</sup> In a previous study we determined that a wide range of epoxy-modified acrylic formulations for 3D printing, the intermediate material was a gel at the end of the first curing stage.<sup>13</sup> This could be expected taking into consideration that the acrylate and epoxy components of this formulation lead to the formation of an interpenetrated network (IPN) structure. In consequence, a solid-like

intermediate material will always be obtained, unless the acrylate component is extremely diluted.

In Figure 7, one can also appreciate the significant increase in the stage 2  $T_g$  with increasing fraction of the CEMA network. Again, this is due to the rigidity of the CEMA network structure and its high  $T_g$ .<sup>19</sup> Taking into consideration the data shown in the figure, for the purposes of our 3D printing tests, we selected HT50CEMA50 formulation, as the printed intermediate material would be a soft gel with a  $T_g$  of -30°C, and the thermally treated (fully cured) part would have a  $T_g$  of 112°C

Figure 7 shows a good agreement between the experimental intermediate  $T_g$  and the one predicted using the Fox expression (Equation 1). However, Figure 7 also shows the experimental  $T_g$ 's of CEMA-rich fully cured materials systematically appear to fall short of the value predicted by the Fox equation. One possible reason might be the occurrence of phase separation leading to a lower concentration of the CEMA network interpenetrated in the polyacrylate network. Given that the sensitivity of DSC might not suffice to observe the glass transition temperatures of different phases, DMA analysis was carried out.

The DMA temperature scan of these materials revealed the presence of two tan delta peaks (**Figure 8**), evidencing phase separation. Given that no visible opacity could be observed in the samples, it is suggested that phase separation occurs in the nano-scale rather than the micro-scale. The first peak corresponds to a softer phase that should be richer in the HT component, while the second peak, appearing at a higher temperature, would be mainly composed of the more rigid CEMA polymer. The lower temperature peak gradually shifts to higher temperatures with increasing CEMA content, while the higher temperature peak hardly changes position. This is even more evident in the loss moduli traces shown in the inset of Figure 8. We determined the  $T_g$  of the soft phase (low  $T_g$ ,  $T_{g,soft}$ ) and the hard phase (hard  $T_g$ ,  $T_{g,hard}$ ) from the tan delta peaks shown in Figure 8. Following the approach of Mezzenga and Månson<sup>22</sup> we used the Fox equation in conjunction with material balances in order to calculate the fraction of the soft and hard phases,  $w_{soft}$  and  $w_{hard}$ , and their composition, expressed in terms of the fraction of HT within the soft and hard phases,  $w_{HT,soft}$  and  $w_{HT,hard}$ . As expected, the results shown in **Table 1** confirm that the main component of the soft phase is HT, although a significant fraction of CEMA can remain solubilized in the soft phase, especially when CEMA content is high. In contrast, the hard phase is predominantly composed of CEMA. The calculated weight fractions

1 of the soft and hard phases agree well with the relative intensities of the tan delta peaks shown  
2 in Figure 8. These results can be rationalized taking into consideration that the HT network is  
3 formed firstly in the photocuring stage of this dual-curing system. In the intermediate material,  
4 the HT network and the unreacted CEMA monomers are perfectly miscible (see **Figure S1** in  
5 supporting information), but the activation of the second polymerization process leads to a  
6 drastic reduction in the entropy of mixing, leading to the segregation of a fraction of the CEMA  
7 network. The presence of a significant fraction of CEMA in the soft phase, promoted by the  
8 compatibilizing H-bonding interactions depicted in Figure 1, is highly beneficial since it shifts  
9 the network relaxation to higher temperatures. This would desirably enhance the mechanical  
10 performance of these materials over the neat HT material.

11 The existence of such phase separation might be beneficial in certain applications where heat  
12 resistance is required. For example, at 150°C, the neat HT100 formulation would be a  
13 completely relaxed rubber (See Figure 8 and **Figure 9**), whereas HT50CEMA50 would still  
14 retain some mechanical strength since the CEMA phase would still not have relaxed at this  
15 temperature. It would therefore be the better choice as a 3D printing resin.

### 26 **2.3. Topology**

27 To investigate the phase separation further, AFM images of the samples were taken, which  
28 corroborated the occurrence of phase separation. Observing the micrographs in **Figure 10**, we  
29 see that the pure formulations HT100 and CEMA100 exhibit nanostructural domains of  
30 approximately 7nm in size, typical of morphologies formed in chain-wise polymerizations.<sup>23</sup>  
31 The nanostructure grows in size up to 20nm in HT25CEMA75 as a function of the CEMA  
32 percentage.

33 This result is in agreement with the two relaxations observed in DMA (discussed  
34 earlier). While one nanophase consists of the main polyacrylate network interpenetrated with  
35 the epoxy-anhydride network, the other is the epoxy-anhydride network partially segregated.  
36 Whereas the former phase would relax at intermediate temperatures as a function of its CEMA  
37 content, the latter would relax at practically the same temperature as a pure CEMA network.

### 38 **2.4. Mechanical performance**

39 As discussed before, 3D printed parts using purely acrylic formulations often fail to meet  
40 mechanical property requirements in advanced applications. Our hybrid acrylate-epoxy  
41

1 formulations are expected to remedy this with their significantly higher  $T_g$  and their more rigid  
2 network structures. We selected HT50CEMA50\_R0,25\_DMAP0,025 and carried out  
3 compression tests following the standard outlined in the Materials and Methods section. To  
4 compare, we also tested neat HT100 specimens (without LUP). For good reproducibility, 3 or  
5 4 specimens were tested for each formulation. Young's Moduli were calculated from the linear  
6 region of the stress-strain relation. Results are given in **Figure 11**. As can be seen, a high level  
7 of reproducibility was achieved.

8  
9  
10  
11  
12 The addition of LUP to the neat formulation and thermally treating the printed specimen  
13 resulted in a 300% increase in Young's Modulus as can be seen. The modulus increases from  
14 an average value of 185 MPa to 700 MPa. This stresses the detrimental effect of non-uniform  
15 degree of cure on the overall mechanical strength of the cured parts. However, the HT100  
16 material cured with LUP still has a limited rigidity given that network relaxation may be taking  
17 place. In contrast, adding 50% (w/w) CEMA increases the Young's Modulus up to 1.9 GPa, a  
18 further 150% increase. The combined effect of LUP and CEMA is a Young's modulus increase  
19 by one order of magnitude (900%), showing the typical stress-strain behaviour of a rigid and  
20 unrelaxed material, in contrast with the printed HT100 material. Considering that the fully cured  
21 neat epoxy-anhydride material has a previously documented Young's modulus of 2310 MPa<sup>19</sup>,  
22 with only 50% of added CEMA, about 73% increase of modulus is already achieved over the  
23 fully cured neat acrylate.

## 24 25 26 27 28 29 30 31 32 33 34 35 36 37 **2.5. Storage Stability**

38  
39 From a practical viewpoint, the long-term storage stability of liquid resins is crucial. To be able  
40 to formulate a one-pot system, the constituents must be chemically stable for long periods. In  
41 this section we present the results from our 2-month stability tests. We kept samples of uncured  
42 HT50CEMA50 containing LUP in an oil bath at 30°C in a dry environment (using moisture  
43 absorbers) and monitored the daily evolution of residual polymerization heat. It is crucial to  
44 maintain dry storage conditions since humidity might cause hydrolysis of the anhydrides to  
45 acids, which in turn would disrupt the stoichiometry and affect the final properties of the  
46 materials. In an attempt to prolong the stability period, we also tested a formulation that  
47 contained the latent base (BG) instead of the pristine DMAP. It was verified by DMA that the  
48 materials obtained using the two catalysts are identical (See **Figure S3** in supporting  
49 information).

1 The stability was monitored by performing dynamic DSC scans on samples on a daily basis and  
2 calculating residual heat and  $T_g$ . The reaction heat of Stage 1 remained unchanged throughout  
3 the 2-month test period. However, the reaction heat of Stage 2 decreased slightly (**Figure 12**),  
4 thereby suggesting the stability was affected, albeit slightly, only by epoxy-anhydride reaction.  
5  
6  
7

8  
9  
10 Despite the fact that formulating with BG increases the epoxy-anhydride reaction onset  
11 temperature, its contribution to stability is minor. As a matter of fact, stability is already quite  
12 good even with DMAP. As can be seen in **Figure 13**, formulations containing either DMAP or  
13 BG are fully stable during the first 15 days. A slight decrease in residual heat (circles) and a  
14 slight increase in  $T_g$  (squares) is observed afterwards. In either case, after 2 months, the  
15 formulations are still far from their gel points and as such, still apt for 3D printing. However,  
16 the conversion of epoxy, albeit limited, might have a certain impact on acrylate network  
17 formation, on the phase separation behavior and ultimately on final material properties.  
18 Investigation of this could prove beneficial for applications with strict property requirements.  
19 Similar to the case with DMAP, it was verified that the loss of stability was mainly caused by  
20 a very slow epoxy-anhydride reaction taking place, due to the limited latency of the initiator. If  
21 activation of the acrylate radical homopolymerization process had taken place, early gelation  
22 might have taken place, rendering the formulations unusable after storage. It can therefore be  
23 argued safely that LUP does not jeopardize the storage stability of the dual formulations.  
24  
25  
26  
27  
28  
29  
30  
31  
32  
33  
34  
35  
36  
37

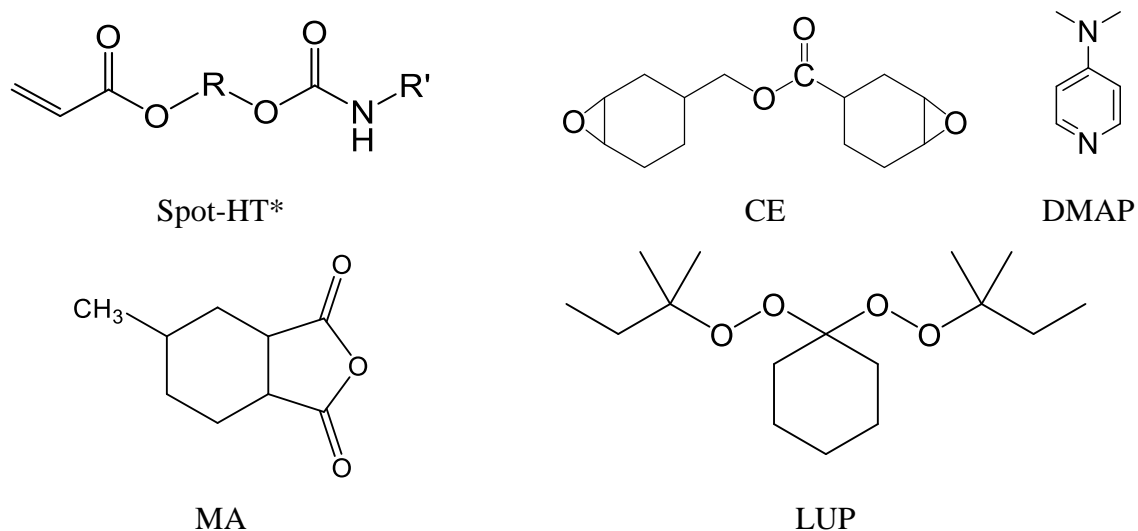
### 38 **3. Conclusion**

39  
40 Photopolymerizable preparations based on acrylates usually suffer from poor mechanical  
41 properties. In this work, we modified such a commercial resin by adding epoxy functionality to  
42 it. Objects are manufactured using a two-step process: a visible light 3D printing followed by  
43 thermal curing of the epoxy-anhydride. By the use of a thermally triggered radical initiator, we  
44 also ensure full acrylate conversion which is otherwise not achievable by photopolymerization  
45 alone within a practical timeframe. DMA revealed bimodal tan delta and loss modulus peaks  
46 and thus indicated phase separation. AFM corroborated this finding and established nanoscale  
47 domains consisting of the main IPN and a separated epoxy-rich phase. Compression tests  
48 revealed that the addition of epoxy-anhydride, together with LUP brought about a 900%  
49 increase in Young's modulus. Coupled with long-term storage stability, these remarkable  
50  
51  
52  
53  
54  
55  
56  
57  
58  
59  
60  
61  
62  
63  
64  
65

findings suggest that these hybrid formulations can be efficiently 3D printed and used in advanced applications requiring superior mechanical performance.

## Experimental Section

The photocurable resin preparation, with trade name Spot-HT (hereafter referred to as HT) (Spot-A Materials), of average molecular weight 648 g and of average functionality 2.26 and of viscosity 350 mPa.s, is a mixture of multifunctional aliphatic and urethane acrylates and a photoinitiator which has an absorption range in the UV-visible region (exact formulation not disclosed by the supplier). The cycloaliphatic epoxy resin was 3,4-epoxycyclohexylmethyl - 3',4'-epoxycyclohexanecarboxylate (CE), with trade name CYRACURE UVR-6105 (IGM Resins) with an epoxy equivalent of 130 g/eq, and a manufacturer specified viscosity of 300 to 450 mPa.s. The anhydride curing agent was Hexahydro-4-methylphthalic anhydride (MA) with a molecular weight of 168.19 g/mol (Sigma Aldrich). The radical initiator was *1,1*-Di(*t*-amylperoxy)-cyclohexane with trade name LUPEROX 531M60 (hereafter, LUP) (ARKEMA). As thermal initiators for the epoxy-anhydride reaction, either the neat 4-dimethyl aminopyridine (DMAP) (Sigma Aldrich) or its tetraphenyl borate salt which is referred to as the base generator (denoted as BG) was used. This base generator was synthesized following the simple mixing-precipitation-filtration-drying procedure outlined in the literature.<sup>24</sup> In **Figure E1**, the structures of all chemicals are given, together with the liberation scheme of the base generator.



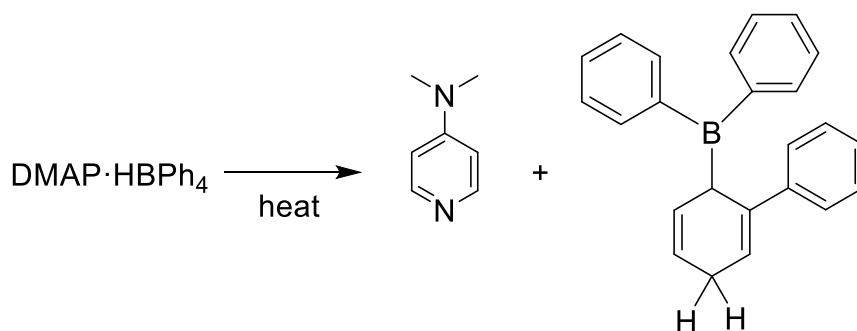


**Figure E1.** Chemicals used in the work. The liberation of the free DMAP from the salt is given at the bottom. \* Exact structure not disclosed by the supplier.

For preparation of the hybrid formulations, firstly a stoichiometric epoxy-anyhdride mixture, denoted as CEMA, was prepared. This was mixed at different rates with the Spot-HT resin to obtain formulations denoted as HTxCEMAy, where  $x$  and  $y$  represent weight fractions of Spot-HT resin and CEMA mixture, respectively. Three formulations were prepared: HT25CEMA75, HT50CEMA50 i HT75CEMA25. The initiator weight percentages were held fixed at 0.25% LUP, and 0.025% DMAP (or 0.5% pel BG) based on total solids. Since the amount of initiators were small, they were added **firstly** to glass vials to facilitate precise sampling. The rest of the components were added subsequently with their weight adjusted according to the amount of initiator weighed. The vials were either immediately sent to analysis, or tightly sealed and stored in a deep freezer at  $-20\text{ }^{\circ}\text{C}$  to avoid penetration of light or humidity and premature activation of the reaction. Some quantity of neat Spot-HT and CEMA formulations were also kept (and denoted as HT100 and CEMA100, respectively) to later analyze and compare them with the hybrid formulations.

For calorimetric measurements, we used a DSC 3+ calorimeter with built-in refrigeration (down  $-80^{\circ}\text{C}$ ) for temperature scans (Mettler Toledo, Barcelona, Spain) and a DSC821 UV calorimeter equipped with a Hamamatsu LC-5 Hg-Xe lamp for photocuring experiments at  $30\text{ }^{\circ}\text{C}$ . The spectral emission range of the UV lamp was 200-600 nm (high intensity around 365 nm). The irradiation intensity was  $21\text{ mW cm}^{-2}$ . Both calorimeters work with a nitrogen purge to ensure an inert atmosphere. Conversion  $x$  could be calculated from calorimetric data using the following expression:

$$x = \frac{\Delta h}{\Delta h_{total}} \quad (\text{E1})$$

Where  $\Delta h$  is the heat released up to a time  $t$  or temperature  $T$ , and  $\Delta h_{total}$  is the total heat released in the experiment. Heating rate was  $10^{\circ}\text{C}/\text{min}$  for all temperature scans. To account for the heat

1 capacity of photocurable formulations, UV-cured samples were re-scanned under the same UV  
2 irradiation conditions. The resulting heat flow curves were subtracted from the original (UV-curing)  
3 curves and analyzed.

4 Dynamic mechanical analysis (DMA) was used to obtain storage modulus and tan delta curves  
5 of intermediate and final materials. The dimensions of test specimens were  $1 \times 13 \times 20 \text{ mm}^3$  and  
6 they were prepared using the following curing procedure: Liquid formulations, except  
7 CEMA100 were injected in transparent glass molds and photocured in a UV oven  
8 (VilberLourmat UV Bio-Link BLX). Each sample received an irradiation of approx.  $2 \text{ J cm}^{-2}$ ,  
9 sufficient for full acrylate conversion. Later, the samples were thermally treated in a Memmert  
10 natural convection oven at  $180 \text{ }^\circ\text{C}$  for 2 hours, and then at  $250 \text{ }^\circ\text{C}$  for another 30 minutes to  
11 ensure full cure. The neat epoxy material, namely CEMA100 was cast in an iron mold with the  
12 same dimensions, and thermally treated with the same procedure described above. Tests were  
13 performed with a TA Instruments DMA Q800 device (TA Instruments, New Castle, DE, USA)  
14 using single cantilever clamp at a frequency of 1 Hz and 0.05% strain, in a temperature range  
15 sufficiently wide to allow a full observation of network relaxation. Heating rate in all DMA  
16 scans was  $3 \text{ }^\circ\text{C min}^{-1}$ .

17 Fourier transform Infrared Spectrometry (FTIR) was used to qualitatively verify conversion of  
18 acrylate and epoxy groups. The FTIR spectrometer was a Bruker Vertex 70 (Bruker Optics  
19 Inc., Billerica, MA, USA) equipped with an attenuated total reflection (ATR) accessory  
20 (GoldenGate<sup>TM</sup>) (Specac Ltd., Orpington, UK) and with a temperature control unit. The  
21 photocuring reactions were carried out in this FTIR by using the same Hamamatsu LC-5 Hg-  
22 Xe lamp at the same irradiation intensity.

23 The conversion of reacting groups were monitored using the Beer-Lambert law and by  
24 normalizing spectra with respect to a reference band. For the photocuring stage, the absorption  
25 band at  $1730 \text{ cm}^{-1}$  corresponding to C=O carbonyl stretch of the ester groups was used as  
26 reference. For the epoxy-anhydride curing, it was the band corresponding to C-H stretching at  
27  $2965\text{-}2850 \text{ cm}^{-1}$ . The general equation to calculate conversion is given in equation 1, where  $A^i$   
28 is the absorbance of the band of interest ( $i=810, 1400$  or  $1636\text{-}1620 \text{ cm}^{-1}$  for acrylate,  $1862\text{-}$   
29  $1785 \text{ cm}^{-1}$  for anhydride, and  $894 \text{ cm}^{-1}$  for epoxy groups),  $A^{ref}$ , the absorption band of reference  
30 (either C=O or C-H stretching) and subscripts 0 and  $t$  represent time. The epoxy band at  $894$   
31  $\text{cm}^{-1}$  was analyzed only qualitatively since this is a convoluted band. Out of the three acrylate  
32 bands available for quantitative analysis, the band at  $1407 \text{ cm}^{-1}$  was used. Although not shown,  
33 the other two bands gave practically identical results.

$$x = 1 - \frac{A_t^i/A_t^{ref}}{A_0^i/A_0^{ref}} \quad (E2)$$

An absolute conversion  $x_{abs}$  could also be calculated taking into consideration the contribution of the two curing processes as:

$$x_{abs} = x_1 \cdot f_1 + x_2 \cdot (1 - f_1) \quad (E3)$$

Where  $x_1$  and  $x_2$  are the conversion of the first and second reactions, and  $f_1$  is a weighing factor indicating the contribution of the first reaction (acrylate polymerization) to the global curing process. For a given formulation, it is simply the mass percentage of its HT100 content (i.e.

$$f_1 = \frac{m_{HT100}}{m_{total}}).$$

The 3D printing of the parts was carried out using a visible light projector adapted to the same MIP-SL configuration as in an earlier paper.<sup>13</sup> The wavelength range of the visible light source was 400-680 nm with a maximum light intensity of 52 mw/cm<sup>2</sup>. As seen in **Figure E2**, the setup consists of a resin tank, a construction platform that moves along the z-axis, and a light source (the projector). The stage that carries the parts moves down a preset distance (0.075 mm) once a layer is photocured.

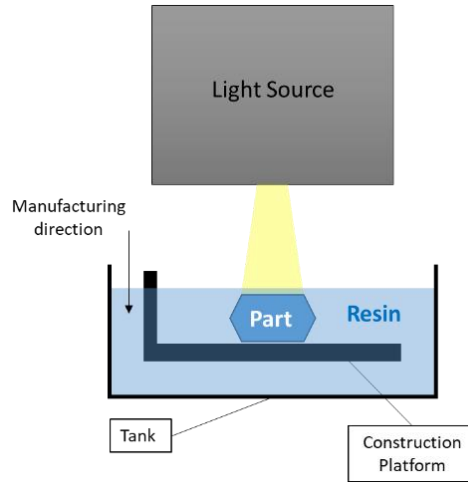


**Figure E2.** Masked Image Processing – Stereolithography (MIP-SL) printer used in the work.

Compression tests were performed on 3D printed neat HT100 and HT50CEMA50 formulations using an Instron 3366 Universal testing Machine (Instron, Barcelona, Spain) according to ASTM D695-15 standard. The nominal dimensions of the test specimen were 12.7x12.7x50.8 mm<sup>3</sup>. The test was performed at a constant displacement rate of 2.6 mm min<sup>-1</sup> until specimen failure or equipment limit (10 kN).

Morphologies of fully cured materials were analyzed using atomic force microscopy. The equipment used was a scanning probe microscope (SPM) (NanoScope IIIa Multimode from Digital Instruments, Veeco Instruments Inc., Plainview, NY, USA) in tapping mode (TM-

1 AFM). One beam cantilever (125 nm) with silicon probe (curvature nominal radius of 5-10  
2 nm) was used. Samples were cut using an ultramicrotome Leica Ultracut R with a diamond  
3 blade.  
4  
5  
6

### 7 **Supporting Information**

8 Supporting Information is available from the Wiley Online Library or from the author.  
9

### 10 **Acknowledgements**

11 The authors would like to thank MCIU (Ministerio de Ciencia, Innovación y Universidades)  
12 (MAT2017-82849-C2-1-R and MAT2017-82849-C2-2-R), FEDER (Fondo Europeo de  
13 Desarrollo Regional) (MAT2017-82849-C2-1-R, MAT2017-82849-C2-2-R and BASE3D) and  
14 Generalitat de Catalunya-Secretaria d'Universitats i Recerca (BASE3D, 2017-SGR-77 and  
15 Serra Húnter program) for the financial support.  
16  
17

### 18 **Conflict of Interest**

19 None to declare.  
20  
21

### 22 **References**

- 23  
24 [1] I.E. Gunduz, M.S. McClain, P. Cattani, G.T.C. Chiu, J.F. Rhoads, S.F. Son, *Addit.*  
25 *Manuf.* **2018**, 22, 98–103. <https://doi.org/10.1016/j.addma.2018.04.029>.  
26  
27 [2] M. Layani, X. Wang, S. Magdassi, *Adv. Mater.* **2018**, 30, 1–7.  
28 <https://doi.org/10.1002/adma.201706344>.  
29  
30 [3] J.P. Rolland, *J. Photopolym. Sci. Technol.* **2016**, 29, 451–452.  
31 <https://doi.org/10.2494/photopolymer.29.451>.  
32  
33 [4] S.C. Ligon, R. Liska, J. Stampfl, M. Gurr, R. Mülhaupt, *Chem. Rev.* **2017**, 117, 10212–  
34 10290. <https://doi.org/10.1021/acs.chemrev.7b00074>.  
35  
36 [5] J.R. Tumbleston, D. Shirvanyants, N. Ermoshkin, R. Januszewicz, A.R. Johnson, D.  
37 Kelly, K. Chen, R. Pinschmidt, J.P. Rolland, A. Ermoshkin, E.T. Samulski, J.M.  
38 DeSimone, *Science (80-. )*. **2015**, 347, 1349–1352.  
39 <https://doi.org/10.1126/science.aaa2397>.  
40  
41 [6] B. Huang, Z. Du, T. Yong, W. Han, *J. Wuhan Univ. Technol. Mater. Sci. Ed.* **2017**, 32,  
42 726–732. <https://doi.org/10.1007/s11595-017-1659-x>.  
43  
44 [7] C. Esposito Corcione, R. Striani, F. Montagna, D. Cannoletta, *Polym. Adv. Technol.*  
45 **2015**, 26, 92–98. <https://doi.org/10.1002/pat.3425>.  
46  
47 [8] S. Lantean, I. Roppolo, M. Sangermano, C. Fabrizio Pirri, A. Chiappone, *Inventions.*  
48 **2018**, 3, 1–13. <https://doi.org/10.3390/inventions3020029>.  
49  
50 [9] J.D. Cho, J.W. Hong, *J. Appl. Polym. Sci.* **2004**, 93, 1473–1483.  
51 <https://doi.org/10.1002/app.20597>.  
52  
53  
54  
55  
56  
57  
58  
59  
60  
61  
62  
63  
64  
65

- 1  
2  
3  
4  
5  
6  
7  
8  
9  
10  
11  
12  
13  
14  
15  
16  
17  
18  
19  
20  
21  
22  
23  
24  
25  
26  
27  
28  
29  
30  
31  
32  
33  
34  
35  
36  
37  
38  
39  
40  
41  
42  
43  
44  
45  
46  
47  
48  
49  
50  
51  
52  
53  
54  
55  
56  
57  
58  
59  
60  
61  
62  
63  
64  
65
- [10] R. Acosta Ortiz, B.A. Puente Urbina, L.V. Cabello Valdez, L. Berlanga Duarte, R. Guerrero Santos, A.E. García Valdez, M.D. Soucek, *J. Polym. Sci. Part A Polym. Chem.* **2007**, 45, 4829–4843. <https://doi.org/10.1002/pola.22234>.
- [11] R. Yu, X. Yang, Y. Zhang, X. Zhao, X. Wu, T. Zhao, Y. Zhao, W. Huang, *ACS Appl. Mater. Interfaces.* **2017**, 9, 1820–1829. <https://doi.org/10.1021/acsami.6b13531>.
- [12] X. Kuang, Z. Zhao, K. Chen, D. Fang, G. Kang, H.J. Qi, *Macromol. Rapid Commun.* **2018**, 39, 1700809/1-1700809/8. <https://doi.org/10.1002/marc.201700809>.
- [13] O. Konuray, F. Di Donato, M. Sangermano, J. Bonada, A. Tercjak, X. Ramis, *Express Polym. Lett.* **2020**, 14, 881–894.  
<https://doi.org/https://doi.org/10.3144/expresspolymlett.2020.72>.
- [14] M. Invernizzi, G. Natale, M. Levi, S. Turri, G. Griffini, *Materials (Basel)*. **2016**, 9,.  
<https://doi.org/10.3390/MA9070583>.
- [15] K. Chen, X. Kuang, V. Li, G. Kang, H.J. Qi, *Soft Matter.* **2018**, 14, 1879–1886.  
<https://doi.org/10.1039/c7sm02362f>.
- [16] J. Bonada, A. Muguruza, X. Fernández-Francos, X. Ramis, *J. Manuf. Process.* **2018**, 31, 689–702. <https://doi.org/10.1016/j.jmapro.2018.01.004>.
- [17] M. Romero, X. Fernández-Francos, X. Ramis, *Polym. Int.* **2019**, 68, 527–545.  
<https://doi.org/10.1002/pi.5743>.
- [18] K. Dean, W.D. Cook, *Macromolecules.* **2002**, 35, 7942–7954.  
<https://doi.org/10.1021/ma020628p>.
- [19] A. Belmonte, F. Däbritz, X. Ramis, A. Serra, B. Voit, X. Fernández-Francos, *J. Polym. Sci. Part B Polym. Phys.* **2014**, 52, 1227–1242. <https://doi.org/10.1002/polb.23555>.
- [20] A. Belmonte, X. Fernández-Francos, À. Serra, S. De la Flor, *Mater. Des.* **2017**, 113, 116–127. <https://doi.org/10.1016/j.matdes.2016.10.009>.
- [21] Z. Doğruyol, F. Karasu, D.K. Balta, N. Arsu, Ö. Pekcan, *Phase Transitions.* **2008**, 81, 935–947. <https://doi.org/10.1080/01411590802136078>.
- [22] R. Mezzenga, J.A.E. Manson, *J. Mater. Sci.* **2001**, 6, 4883–4891.
- [23] D.H. Builes, A. Tercjak, I. Mondragon, *Polymer* **2012**, 53, 3669–3676.  
<https://doi.org/10.1016/j.polymer.2012.06.018>.
- [24] T. Rodima, I. Kaljurand, A. Pihl, V. Mäemets, I. Leito, I.A. Koppel, *J. Org. Chem.* **2002**, 67, 1873–1881. <https://doi.org/10.1021/jo016185p>.

1  
2  
3  
4  
5  
6  
7  
8  
9  
10  
11  
12  
13  
14  
15  
16  
17  
18  
19  
20  
21  
22  
23  
24  
25  
26  
27  
28  
29  
30  
31  
32  
33  
34  
35  
36  
37  
38  
39  
40  
41  
42  
43  
44  
45  
46  
47  
48  
49  
50  
51  
52  
53  
54  
55  
56  
57  
58  
59  
60  
61  
62  
63  
64  
65

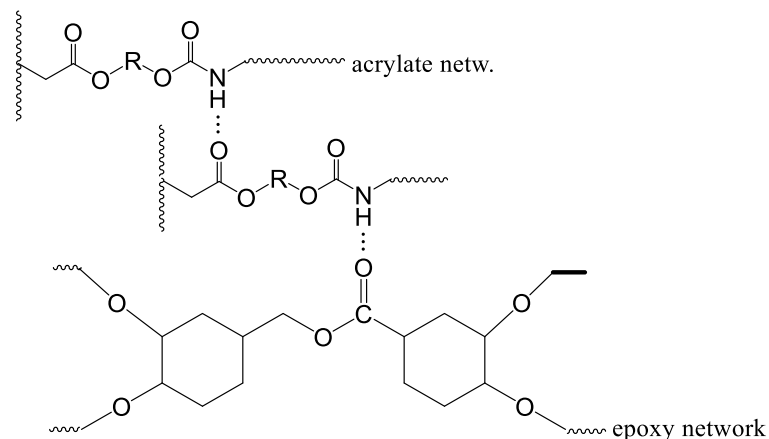


**Figure 1.** Hydrogen bonding interactions within the IPN formed by the two-step curing of hybrid formulations.

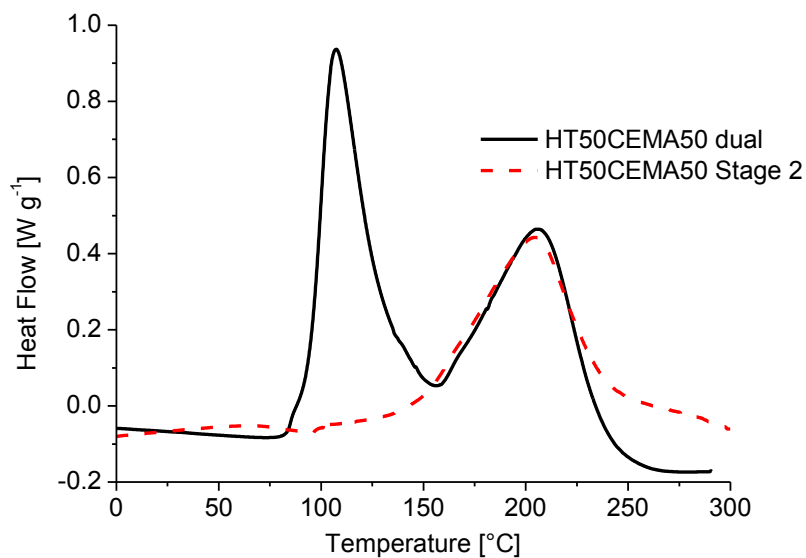


**Figure 2.** DSC thermogram of the overall curing process (black solid line) and the epoxy-anhydride reaction (stage 2) of the same hybrid formulation (red dashed line)

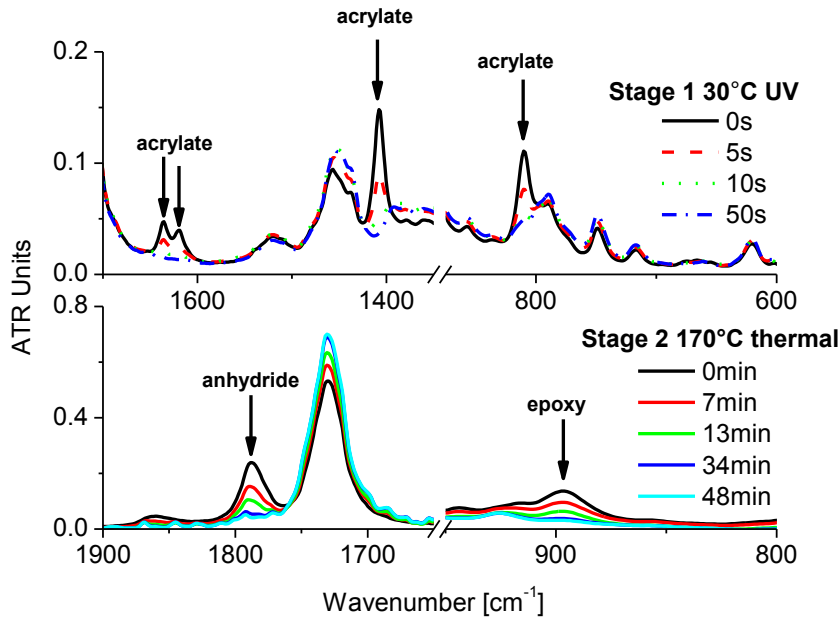


**Figure 3.** Evolution of FTIR spectra during UV curing of acrylates at 30°C (top figure), followed by thermal epoxy-anhydride reaction at 170°C (bottom figure).

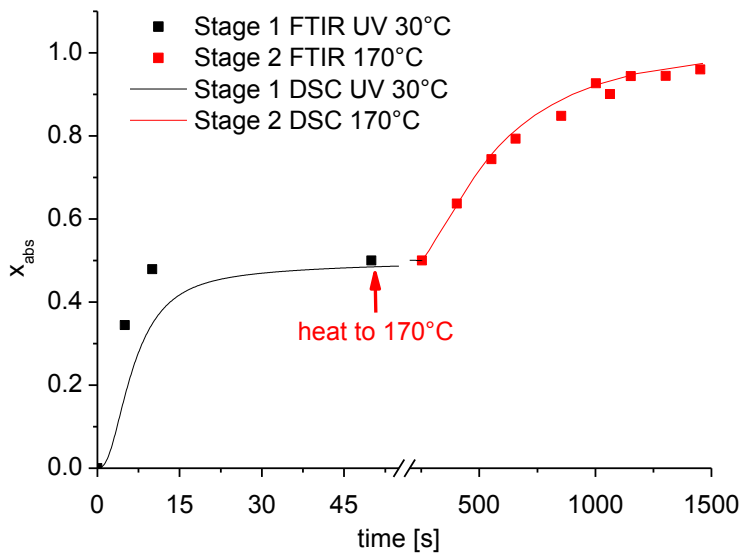


**Figure 4.** Experimental absolute conversions obtained with DSC (continuous) and FTIR (discrete symbols). The monitored conversion was of acrylate and anhydride groups, in stages 1 (UV) and 2, respectively.

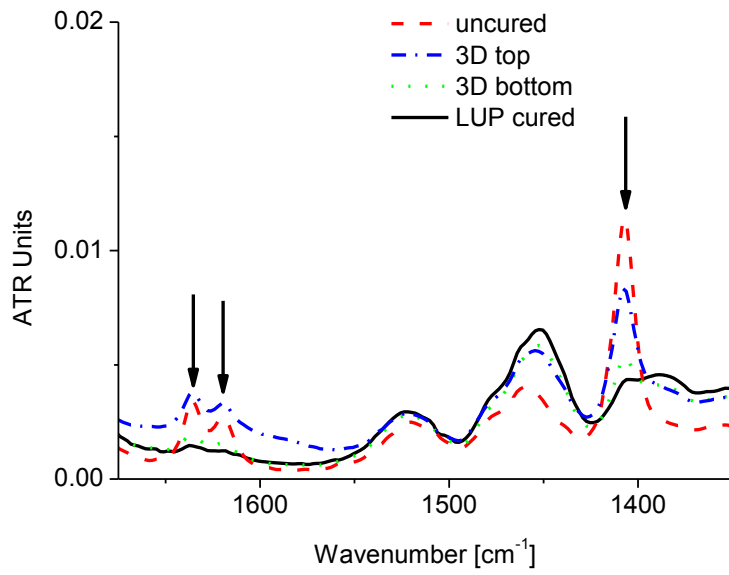


**Figure 5.** FTIR spectra of a 3D printed 1,5mm thick rectangular prism from the HT100 formulation. Use of LUP eliminates inhomogeneity of cure.



**Figure 6.** A 3D printed bust of Albert Einstein. The clearly visible layers had a thickness of 0,075mm each.

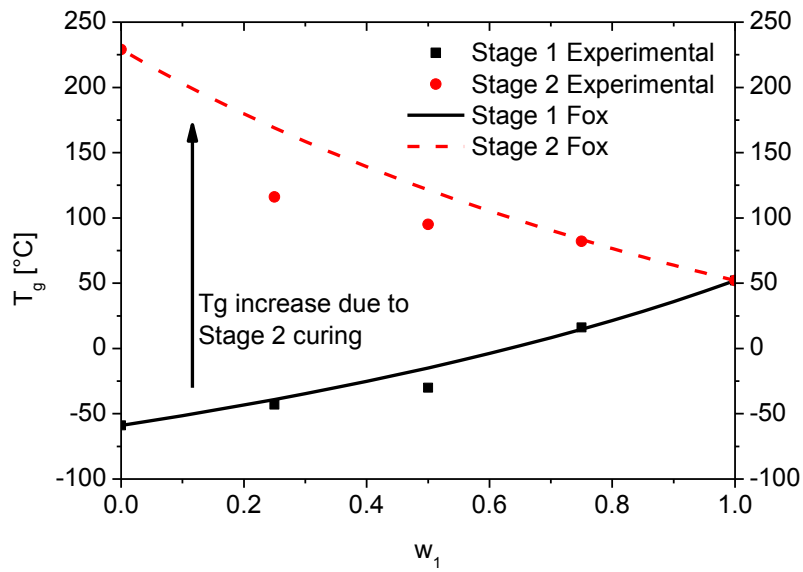


**Figure 7.** Experimental vs. predicted Stage 1  $T_g$  (after photocuring) and Stage 2  $T_g$  (after thermal curing), as a function of HT weight fraction,  $w_1$ . Samples were prepared as explained in the experimental section.

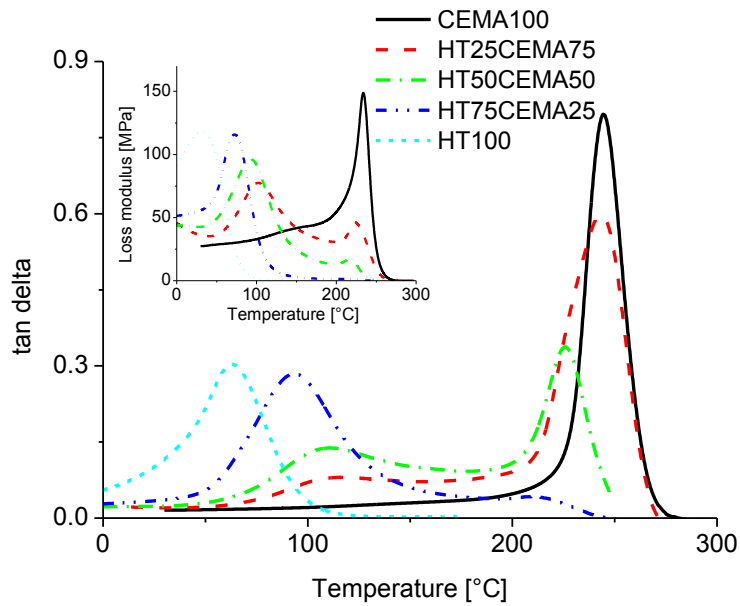


**Figure 8.** DMA tan delta curves of fully cured samples. Inset: Loss moduli.

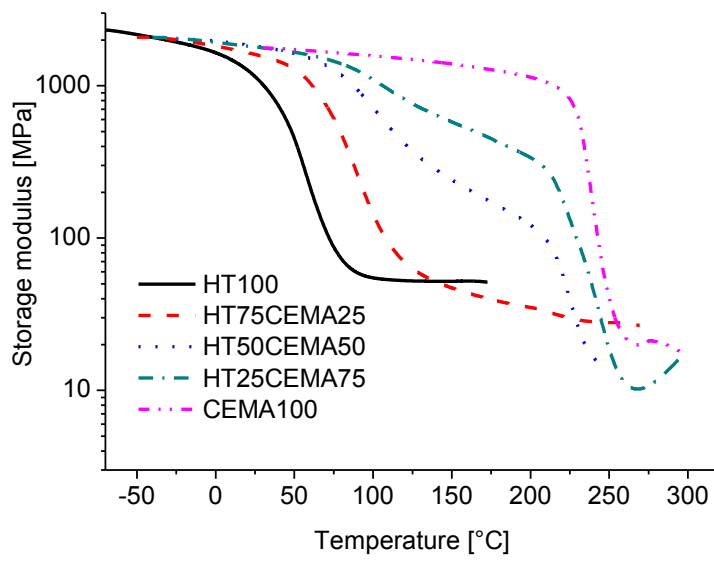


**Figure 9.** Storage moduli of fully cured samples.

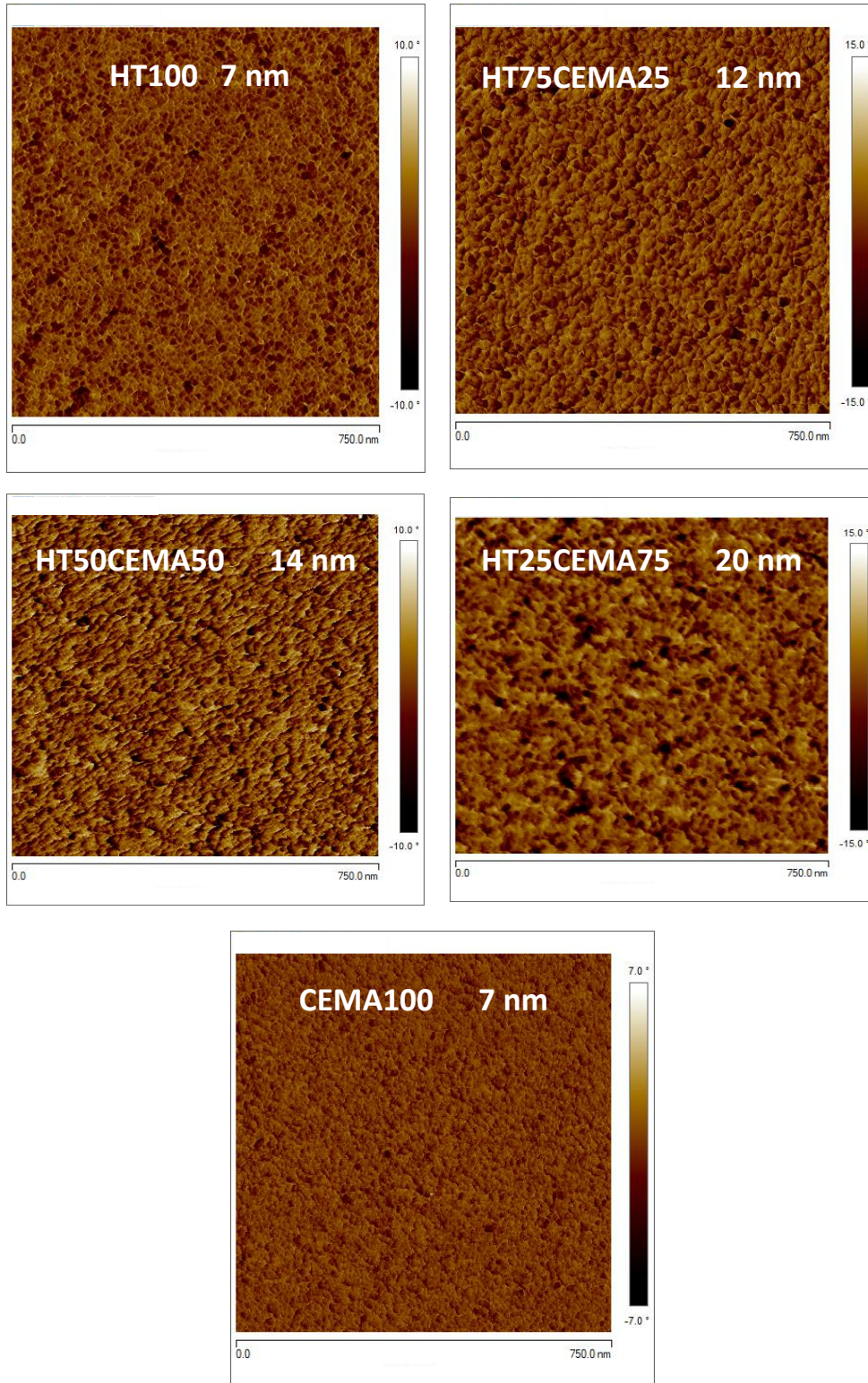


**Figure 10.** AFM phase images of all HT-CEMA hybrid formulations. The phase signal changes when the probe encounters regions of different composition. These phase shifts are registered as bright and dark regions (with their corresponding values in degrees).

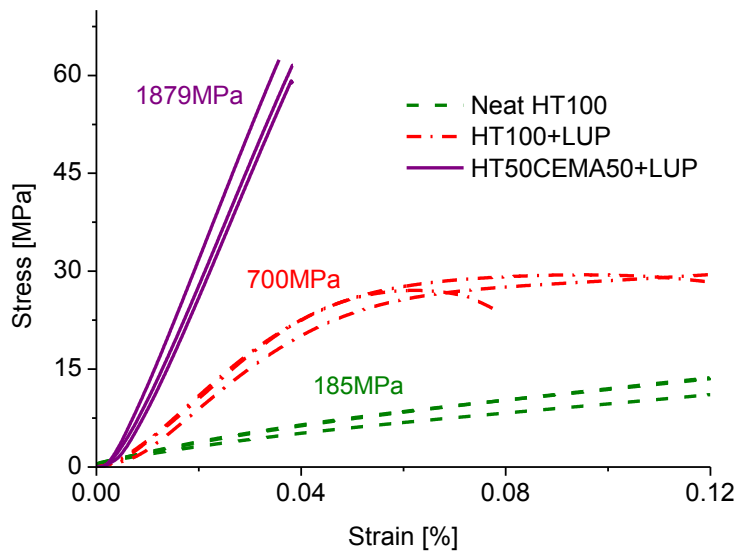


**Figure 11.** Stress-strain curves during compression tests. Young's moduli of epoxy and LUP doped formulations are higher by an order of magnitude compared to their neat counterparts.

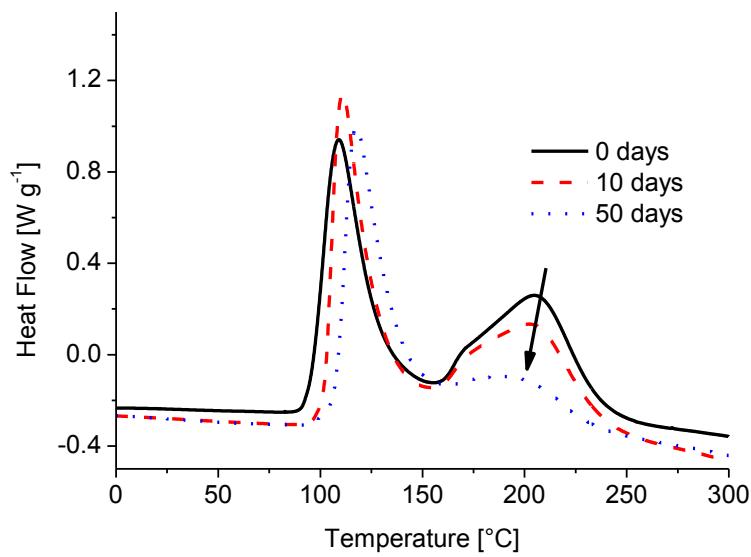


**Figure 12.** 50-day evolution of DSC thermograms of samples stored at 30°C

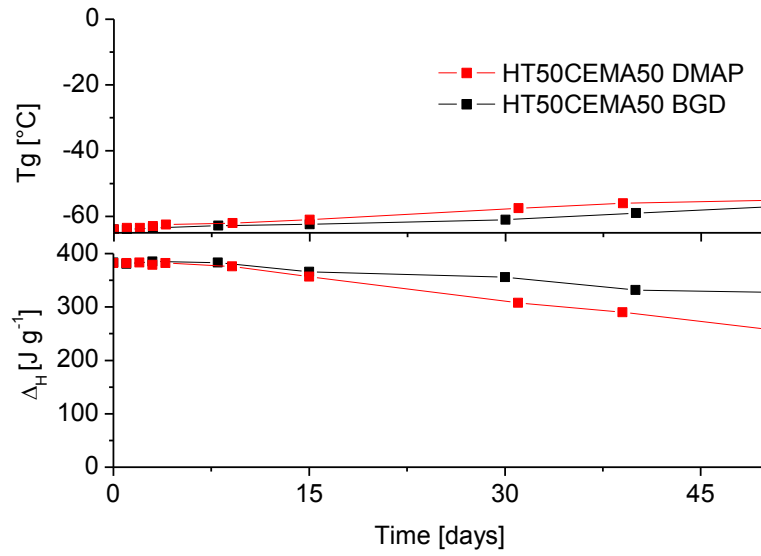
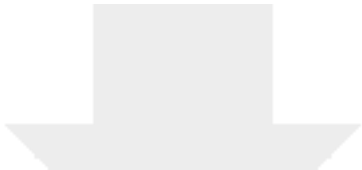


**Figure 13.** Room temperature stability of HT50CEMA50 formulated either with DMAP or BGD. The increase in  $T_g$  (top) and decrease in residual heat (bottom) have no practical significance, suggesting good stability.

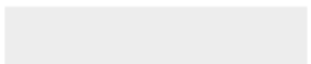
**Table 1.** Fractions and compositions of the soft and hard nano-phases in each formulation

Formulation	$T_{g,soft}$ [°C]	$T_{g,hard}$ [°C]	$w_{soft}$	$w_{hard}$	$WHT_{,soft}$	$WHT_{,hard}$
CEMA100	-	245	-	1	-	0
HT25CEMA75	117	243	0.406	0.594	0.606	0.007
HT50CEMA50	109	225	0.730	0.270	0.657	0.074
HT75CEMA25	94	210	0.985	0.015	0.760	0.134
HT100	63	-	1	-	1	-



Click here to access/download

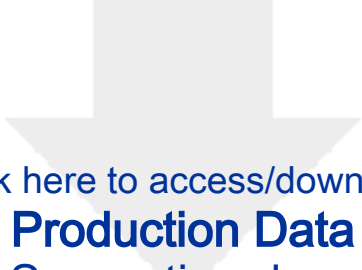
**Production Data**  
Graphical TOC.tiff





Click here to access/download  
**Production Data**  
short summary.docx





Click here to access/download  
**Production Data**  
Supporting.docx

